Journal of Enhanced Heat Transfer, 30(1):35–52 (2023)

NUMERICAL INVESTIGATION ON EFFECT OF TARGET COOLANT DELIVERY IN LIQUID-COOLED MICROCHANNEL HEAT SINKS

Pardeep Shahi,* Apurv Deshmukh, Hardik Yashwant Hurnekar, Satyam Saini, Pratik Bansode, & Dereje Agonafer

Mechanical and Aerospace Engineering Department, The University of Texas at Arlington, Arlington, Texas, USA

*Address all correspondence to: Pardeep Shahi, Mechanical and Aerospace Engineering Department, The University of Texas at Arlington, 500 W 1st St, Arlington, TX 76019, Texas, USA, E-mail: pardeep.shahi@mavs.uta.edu

Original Manuscript Submitted: 5/10/2022; Final Draft Received: 6/29/2022

Rising demand for high-performance processors and increased difficulty in their thermal management have resulted in the need for advanced and efficient cooling technologies like direct-to-chip liquid cooling. Typical CPUs/GPUs today have multiple cores, and at any given time, not all the cores in the package are utilized, which creates a nonuniform heat distribution or a thermal gradient across the processor. This can lead to reliability issues due to localized thermal transients and cyclic thermomechanical stresses. A practical solution to solve this issue is investigated in this paper by proposing a dynamic cold plate and analyzing its thermal performance using computational fluid dynamics (CFD) modeling. The proposed cold plate design consists of four different fin sections. The flow rate to each of these fin sections is regulated passively using bimetallic strips that respond to the outlet temperature of the coolant. A cold plate that can dissipate a maximum of 360 W was first designed and optimized using multiparametric optimization in optiSLang. Based on the anticipated heat loads, a bimetallic strip was selected and analyzed for maximum deflections using finite-element analysis using a range of cold plate operating temperatures. The results show that the proposed cold plate design can reduce the thermal resistance by a maximum of 42%. Furthermore, a maximum reduction of 62% was observed in the temperature difference value of the power sources as compared to the baseline design.

KEY WORDS: *data center, liquid-cooling, electronics cooling, cold plate*

1. INTRODUCTION

Air cooling of servers has proven to be sufficient over the past few decades owing to processors' low thermal design power (TDP), the type of applications, and the nature of workloads. With the end of Dennard scaling and rapidly increasing transistor count, attributed to exceptionally high-performance demands in applications like artificial intelligence (AI) and machine learning (ML), TDPs have started to exceed the air-cooling limits. Keeping up with the demand for high performance, the solution providers have already started resorting to advanced thermal management strategies like single-phase immersion cooling (Niazmand et al., 2020a), two-phase cooling (immersion and cold plate-based) (Hoang et al., 2020; Niazmand et al., 2020b; Kumar

et al., 2018), and single-phase cold plate liquid cooling (Kandlikar and Hayner, 2009; Li and Kandlikar, 2015). All these techniques have their own merits in terms of reduced total cost of ownership (TCO), power scalability, ease of deployment, retrofitting, and enhanced reliability and thermal performance. Some of these studies also discuss the seeding of the primary coolant with nanoparticles to further improve the coolant heat transfer performance (Niazmand et al., 2020; Shahi et al., 2020).

It was pointed out in the early 2000s that the electronic package TDPs were doubling every 36 months, which would lead to very high heat fluxes and surface temperatures at the package level. High temperatures are one of the primary causes of failure in electronics. Studies show that almost 55% of the failures can be attributed to high package temperature (Bailey, 2008; Khattak and Muhammad, 2019; Saini et al., 2022). Other failure modes include humidity and contamination-related failure due to the flow of ambient gaseous and particulate matter inside the data centers under favorable conditions (Saini et al., 2020a,b). Indirect liquid contact-based cold plate cooling outperforms most of the advanced cooling techniques by taking advantage of a higher convective heat transfer coefficient in the micro- and minichannels. Deionized water or water-based glycols are ideal cold plate coolants for high heat flux applications because water has higher thermal mass, which makes it easier to transport large heat fluxes as compared to air cooling. Conjugate heat transfer in cold plates with rectangular mini- and microchannel geometries has been well accounted for in the literature in the form of experimental and numerical studies (Li et al., 2004; Qu and Mudawar, 2002).

It is also noted that not only the temperature but the temperature distribution on the electronic package also plays a key role in package level failures. A shortcoming of traditional cold plates is the nonuniformity of flow distribution inside the microchannels that causes a maldistribution of the flow between the inlet and the outlet (Lu and Wang, 2006). This further increases the risk of failure of critical electronic packages. Other studies (Hegde and Seetharamu, 2008) used numerical modeling to analyze the effectiveness of a two-layered heat sink and concluded that this arrangement gives a lower surface temperature at the chip. It was further verified that partial heating of the flow near the outlet further reduces the thermal gradient on the chip surface (Wei, 2004). The effect of varying the chip layout was studied by Chauhan et al. (2010), where the high heat flux components were placed toward the channel inlet for a better thermal profile on the chip. The effect of three different inlet and outlet manifold arrangements has also been studied (Xie et al., 2014). These manifold geometries considered in this study were inline, diagonal, and perpendicular to the flow direction with two hotspot locations. The results showed that better thermal performance was achieved when the inlet and outlet ports were located in a direction normal to the heat sink surface. At the same time, in terms of hydraulic performance, such an arrangement also leads to higher pressure drops across the cold plates. The FCD design study allows for workload-based allocation of coolant to each server in a rack (Shahi et al., 2022). Similarly, research on an open compute server retrofitted with cold plates and distributed pumps revealed significant power savings when the flow management at the server level is dynamically changed (Shahi et al., 2021). Other studies look into narrowing the channel width at hot spot locations (Prasher and Chang, 2008), using varying channel widths to accelerate the flow over the hotspots (Sharma et al., 2015), increasing channel depth above hotspots to enhance heat transfer area for the fluid (Dias and Skoglund, 2008), locally provisioning higher volume flow rate to hotspot locations (Goodson et al., 2006), and using oblique fins and fin density at hot spot locations (Lee et al., 2010, 2013). Optimized design of cold-plate microchannels using various regression-based schemes has been done using computational fluid dynamics (CFD) to reduce overall thermal resistance and pressure drops (Ariyo et al., 2021).

To address the issue of temperature nonuniformity at the package level, the present investigation proposes a novel cold plate design and analyzes its performance using CFD. This cold plate design passively regulates the flow to the hotspots/sources at the bottom using bimetallic strips integrated within the cold plate. The study discusses the proposed cold plate design development, multiparametric optimization of the cold plate design, thermal analysis of the bimetallic strips, and the improvement of thermal performance as compared to the baseline cold plate design. A detailed discussion is provided on the design and design optimization of the cold plate using multiobjective multiparametric parametric optimization in optiSLang (Ansys, 2019). The cold plate itself is a three-part assembly containing a bottom, middle, and top section as shown in Fig. 1. The bottom part of the plate assembly contains four different sections of parallel copper microchannels. The middle section of the plate has both an inlet and outlet passage for the coolant, and the top section of the plate is the plastic sealed cover plate. The coolant impinges into the center of the bottom section from the middle plate and then moves laterally through the four microchannel sections toward the outlet which is linked to the middle section. The fluid thus keeps recirculating between the middle section and the bottom section of the cold plate. The first part of this paper discusses the CAD design and design optimization of the cold plate. The upcoming sections of the manuscript will discuss the cold plate optimization strategy and analysis of bimetallic strips and their integration with the cold plate design. Finally, the numerical approach to analyze the performance of the optimized cold plate assembly and the discussion of improved thermal performance results are provided.

2. COLD PLATE DESIGN AND OPTIMIZATION

This section will discuss the design approach followed for the dynamic cold plate concept and final design. The approaches discussed include a preliminary approach based on a miniaturized flow control device and the final design approach using bimetal strips. The cold plate fin design

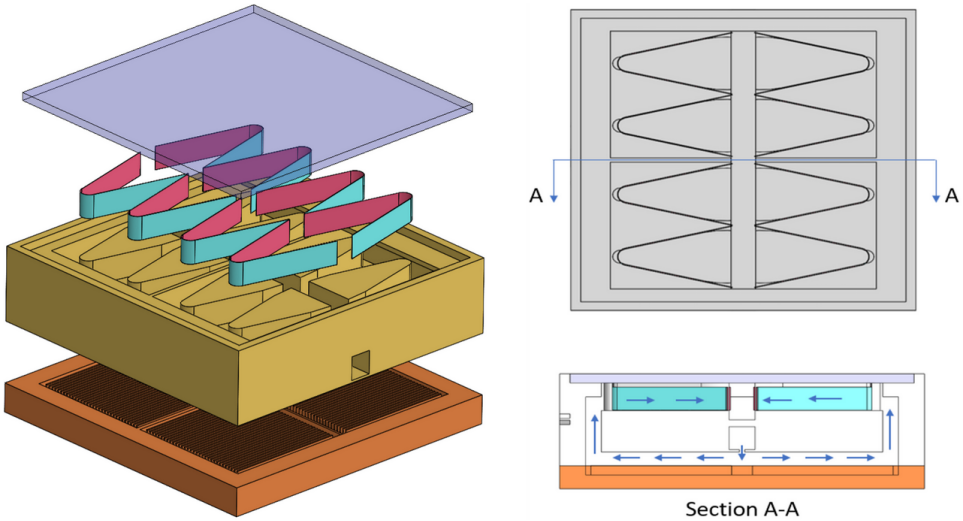

(a) (b)

FIG. 1: (a) Exploded view of the cold plate CAD geometry showing the top, middle, and bottom plates; and (b) sectional view of the cold plate showing the movement of the coolant through various parts inside the cold plate

optimization process and the selection process of the bimetal strip for the final cold plate design are also described.

2.1 Nitinol Spring Approach

Previous work done on the dynamic cold plate by our research group focused on the development of a cold plate design using a self-regulated temperature-sensitive material. In this design, a miniaturized flow control device was made from nitinol, which is a nickel-titanium shape memory alloy that responds to temperature change. This idea of implementing a self-regulated miniatured flow control device (FCD) is discussed in recent literature (Kasukurthy et al., 2018). In this study, the miniaturized FCD is integrated with a nitinol spring that is connected to a damper inside the FCD cavity. Based on the outlet coolant temperature (coming out from the hotter section of the cold plate), the spring deflects the damper, allowing more coolant to enter that section of the cold plate. Thus, the device proposed the idea of improved temperature distribution on the processor case. The major bottleneck in the design and development of this device was the lack of material reliability data as well as difficulties in miniaturizing the device so it can be integrated inside a cold plate successfully. Thus, the authors decided to integrate bimetallic strips with the cold plate design that addresses the material reliability, miniaturization, and any related operational issues. Further details about the new cold plate design are discussed in the upcoming sections.

2.2 Cold Plate Fin Optimization

Liquid cooling using cold plates for high-performance computing servers has gained a lot of momentum, and significant attention has been paid to optimizing the cold plate performance. Traditional cold plate designs for data center applications comprise parallel mini- or microchannel fins embedded inside a cavity. These fins are typically made up of copper. With water-based coolants, cold plates typically offer a very high value of convective heat transfer coefficients. Significant efforts are made to optimize the manufacturing processes and design geometries of the cold plate fins to improve the heat transfer and reduce cold plate pressure drops. For the current cold plate design, Ansys optiSLang (Ansys, 2019), a commercially available design optimization tool, was used to optimize the baseline cold plate geometry.

The baseline design of the cold plate is divided into three main subassemblies. The middle plate assembly of the cold plate is modified in such a way that the V-shaped bimetal can be fitted into it and flow leakage is avoided. For that purpose, the supporting V-shaped structures are patterned as shown in Fig. 1. The gap between two supporting structures acts as a fluid path and can be regulated with help of the bimetal deflection. The bottom of the middle plate has a slit to enter the water into the fins as shown in the figure. The bottom cold plate is divided into four identical fin sections that are separated to avoid the mixing of the hot and cold fluid streams. The flow path of the coolant in the typical single inlet and single outlet cold plates with parallel channels results in nonuniform flow. This is primarily due to the jetting action of fluid at the entrance of the microchannel passage. Providing the inlet in the middle of the cold plate and the sectioning of the fin cavity results in a more uniform flow distribution through the fin cavity, as will be shown in the results section. The thickness of the entire cold plate assembly is maintained close to 22 mm to meet the space constraints for final assembly within a 1U server. The fin passages and inlet and outlet are kept perpendicular to the flow direction as shown in the complete 3D CAD model in Fig. 1. The baseline design of the cold plate operates like the traditional cold plates, but the fin

cavity is optimized for the best thermal and hydraulic performance using multivariable design optimization. For optimization of the cold plate fin cavity, the objective functions that control the geometry optimization of the fin parameters were minimizing the pressure drop and reducing the temperature difference between the cold plate inlet and outlet. The variables parametrized in the optimization and their optimization range are as follows:

- Fin thickness: 0.1–1 mm.
- Fin spacing: 0.2–1 mm.
- Inlet velocity: 0.029–1.91 m/s.

Baseline steady-state thermal simulations of the cold plate are run using Ansys Icepak (2019), in which the input parameters for optimization are provided as input and the objective functions are defined. These design variables and objective functions are integrated with optiSLang, where the design points are generated based on the range of the defined variables/design parameters. The objective functions set for the current optimization study were minimum pressure drop and minimum source temperature below the cold plate. Each of these generated design points is then iteratively run in Icepak and the results of the objective function values are generated. A summary of the results of optimized design points for the objective functions of minimum pressure drop and source temperature values is shown in Fig. 2. Figure 2 is a Pareto plot where each black dot represents the solution of a design point of the optimization study. The design points shown on this graph depict the best values of the fin parameters for which both the pressure drop and the temperature difference are minimum. The final optimized CAD of the old plate bottom plate is shown in Fig. 3. Based on the obtained data, the best values of the fin parameters are as follows:

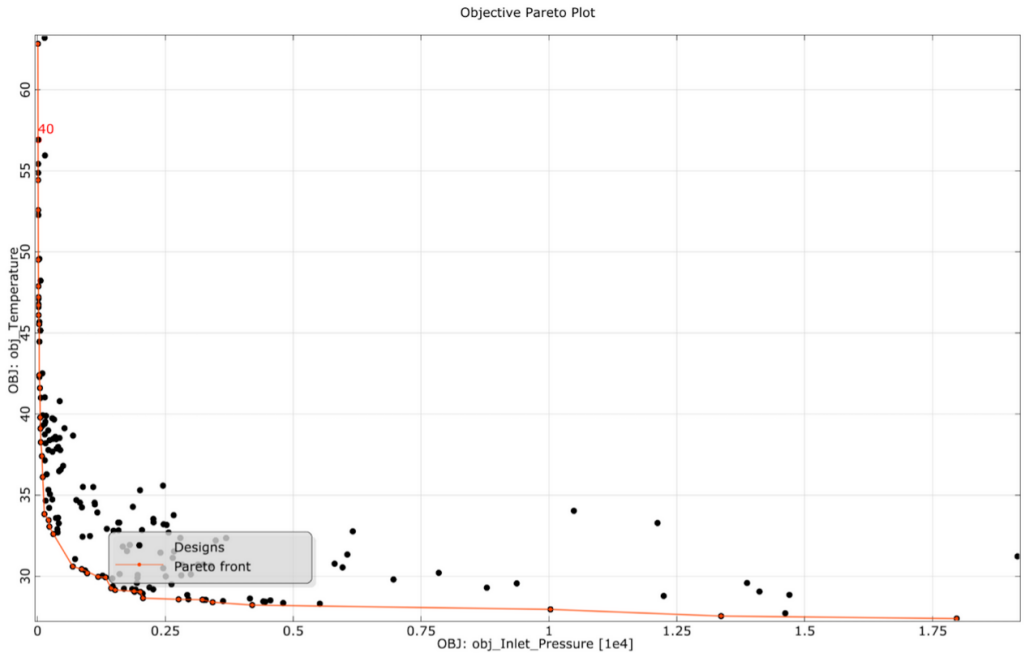

FIG. 2: Pareto plot showing the values of the objective functions (temperature and pressure drops) for various design points simulated during multiobjective optimization

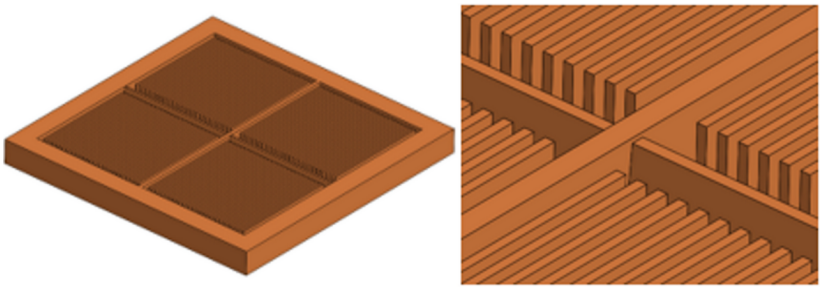

FIG. 3: CAD model of the optimized fin geometry showing the four fin sections in the bottom plate of the cold plate

- Fin thickness: 0.48 mm.
- Fin spacing: 0.48 mm.
- Inlet velocity: 0.4 m/s.
- Inlet pressure: 135.46 Pa.
- Maximum temperature: 33.83°C.

2.3 Bimetallic Strip Approach

The next step was to integrate the bimetallic strips within the cold plate design. Before this, a detailed analysis of the bimetallic strip was done to quantify the amount of deflection bimetal will undergo based on the anticipated outlet temperature from each section of the cold plates. *Bimetal* is a composite material and is usually found in the form of a sheet or a strip. It is manufactured with a special engineering technique that involves the bonding of two or more metallic layers having different coefficient of thermal expansion (CTE) values. As the temperature at the strips varies, both the materials expand or contract differently causing a deflection as shown in Fig. 4. This property of the bimetal, also known as thermostatic material, is widely used. These materials are employed in many industries including automotive, HVAC, space science, and even the military. The deflection of the bimetal is directly proportional to the CTE and working

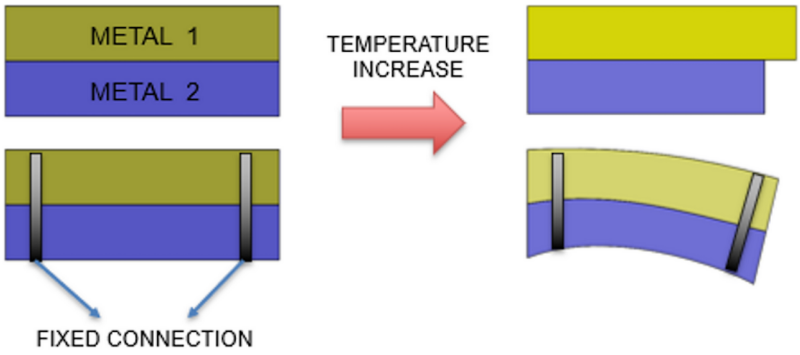

FIG. 4: Overview of the working principle of bimetal strip showing the deflection due to temperature increase (based on the results)

temperature and inversely proportional to the total thickness of the strip. It is also a function of the modulus of elasticity of both the materials and their thicknesses.

The V-shaped bimetallic strips are located in the middle plate of the cold plate assembly, where warm coolant returns from the bottom plate. These bimetallic strips deflect based on the outlet temperatures from different fin sections at the bottom, thus varying the volume flow rate passing through them. When the temperature of the coolant coming out from any of the four sections rises due to a local increase in heat flux from the processor region below the cold plate, the bimetallic strip for that region will respond by increasing the percentage of open area for more coolant to flow through it. At the same time, if other regions on the processor are experiencing low localized heat flux, the bimetallic strip for that section will deflect and partially close, thereby reducing the coolant flow rate to that section. This process will thus reduce the overall temperature gradient over the surface of the processer, unlike traditional cold plates.

2.4 Bimetallic Strip Deflection Analysis

Many bimetal materials are available in the market that can be selected as per the deflection requirements specific to the application. The deflection of these materials is based on two material properties: thermal expansion coefficient and flexivity. Flexivity is the factor that defines both CTE and deflection. Table 1 shows the list of the bimetals that have been referred to from the EMSclad bimetal manufacturer for selection for the cold plate design. Out of several available bimetals, GB14 is a two-layer bimetal in which alloy GB has 10.2×10^{-6} F-1 CTE and alloy 14 has 3.5×10^{-6} F-1. To accommodate the bimetal strips into the cold plate, a V-shaped bimetal geometry was chosen because it allows a larger bimetal strip length. This is because the bimetal deflection is directly proportional to the thickness of the layer. Therefore, a larger length of the bimetal will result in a higher deflection. To obtain the optimum length, thickness, and deflection combination for the bimetal strips, steady-state thermal simulations were done. As shown in Fig. 5, a steady-state thermal loading from 25°C to 70°C in ten-step intervals is provided to V-shaped bimetallic strips. The material properties were directly referred to from the company data sheet and imported to the Ansys engineering materials list. A rectangular mesh of around

TABLE 1: List of the Bimetal from EMSclad data sheet (Engineered Material Solutions, 2021)

Material type	ASTM flexivity, F $\times$ 10^{-7}	Maximum sensitivity temp., °F	Deflection temp. range, °F	Modulus of elasticity, E	Resistivity	Density	ASTM type
F7OR	147	0 to 300	–100 to 500	24.5	70	0.299	TM27
F9OR	148	0 to 300	–100 to 500	25.0	90	0.298	TM28
F100R	149	0 to 300	–100 to 500	25.0	100	0.297	—
F125R	148	0 to 300	–100 to 500	25.0	125	0.297	—
F55R20	130	100 to 500	–100 to 700	22.0	54	0.300	—
G7	61	0 to 800	–100 to 1000	27.5	440	0.280	—
GB2	128	100 to 550	–100 to 1000	26.0	445	0.295	—
GB5	75	300 to 800	–100 to 1000	26.0	342	0.296	—
GB14	100	0 to 300	–100 to 1000	26.0	511	0.294	—
J1	134	0 to 300	–100 to 500	19.0	110	0.310	—
J7	56	0 to 500	–100 to 500	22.0	106	0.300	—
LA1	158	0 to 300	–100 to 700	25.0	475	0.292	TM29

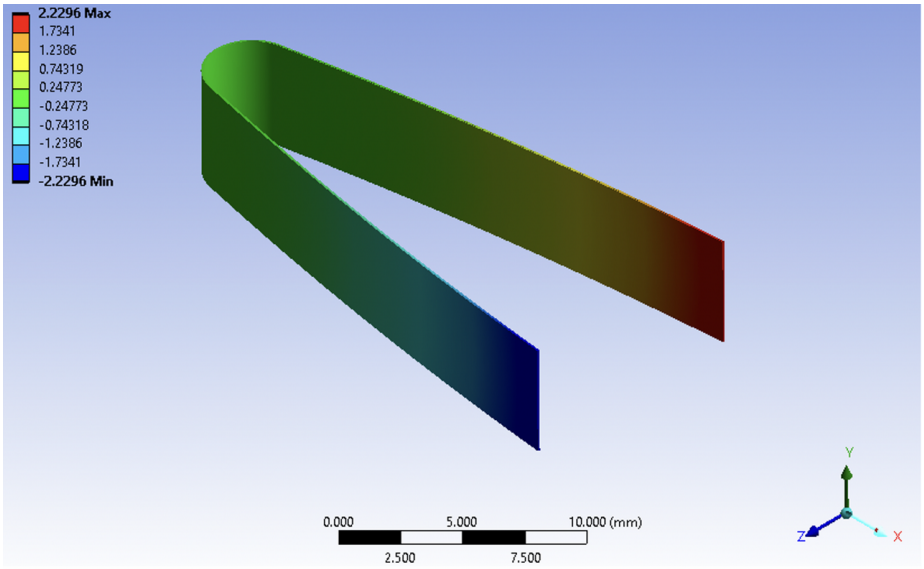

FIG. 5: GB14 deflection (z-axis) in V shape. 50 mm length and 0.1 mm thickness.

79,002 elements and 559,920 nodes with an element size of 0.08 mm was created for the bimetal. Table 2 shows the mesh sensitivity analysis of the bimetal strip for thermal simulations. By using such geometry, relatively longer bimetal strips can be adopted into a cold plate. Figure 6 represents a comparative study of length and relative deflection in mm.

3. COMPUTATIONAL MODELING

Since it is extremely difficult to simulate a three-way fluid-structure-thermal interaction using CFD, steady-state simulations of the cold plate assembly with bimetals were done in Ansys Icepak (2019). The total deflections of the bimetal strip were first calculated using steady-state thermal simulations as discussed previously. The CFD was then run as separate cases by using the deflection values from the steady-state simulations and the improvement in temperature drop

TABLE 2: Mesh sensitivity study for (top) bimetal steady-state thermal simulation and (bottom) cold plate thermal simulation

Number of elements	Max. deflection at 70°C
45,236	2.054 mm
79,002	2.2296 mm
120,120	2.2297 mm
145,638	2.2298 mm
Number of elements	**Thermal resistance at 0.6 lpm (°C/W)**
126,098	0.041
341,732	0.036
695,713	0.034
1,186,324	0.034

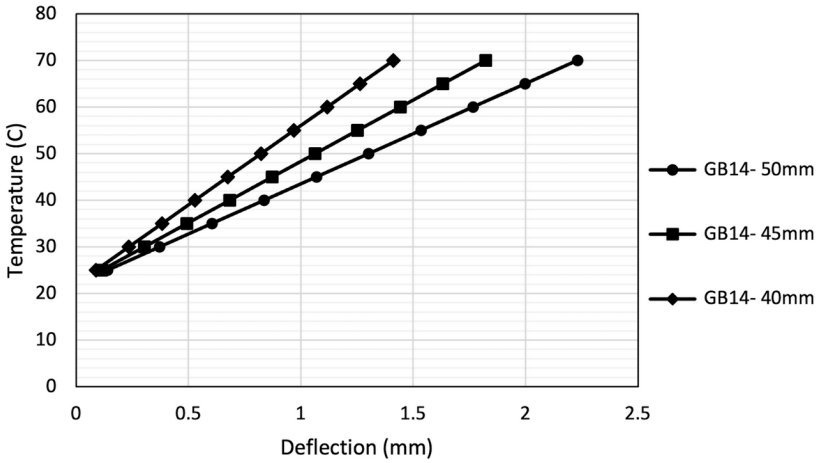

FIG. 6: Comparison between the different lengths of the bimetal to respective deflection

across the cold plate was calculated for each of these cases in Icepak. This was done by manually modeling blocks (where the bimetal is located) to create the same effect as in the case of bimetal deflection corresponding to different coolant temperatures. Each of these blocks represents one end of the bimetal, and as the directional deformation of the bimetal is known, a precise opening length can be given for different cases of coolant temperature. As an example, if the temperature in a specific section of the cold plate is 45°C and the corresponding bimetal directional deflection is 1.2 mm, a value of 1.2 mm is used as an open length and the rest is blocked. The exact values of the temperatures at the bimetal have been obtained from the simulation case where no bimetal is present.

The quality of the mesh in the CFD study defines the quality of the results, and good quality and optimum element count mesh are characterized by grid-independent results. For conjugate heat transfer problems, as in this case, care should be taken to have a sufficient number of nodes on the fluid region between the fins and on the solid as well. To achieve this, per-object meshing properties are applied to all the fins where a user-defined number of elements is selected in the x-, y-, and z-directions of the fins and also the fluid regions. Figure 7 represents meshing on the fins. For the global geometry, a minimum mesh element size was set to 0.04 mm and around 1.58 million elements were produced.

For this study, laminar flow equations were considered as the flow regime inside the inlet, outlet, and cold plate fins remain laminar. Listed subsequently are the governing equations used by the software to generate a converged solution.

Mass conservation:

$$\frac{d\rho}{dt} + \nabla.(\rho v) = 0 \tag{1}$$

Momentum conservation:

$$\frac{d}{dt}(\rho v) + \nabla.(\rho v v) = -\nabla P + \nabla(\tau) + \rho g \tag{2}$$

In the preceding equation, P is referred to as static pressure, ρg is known as body force due to gravitation, and τ is the stress tensor.

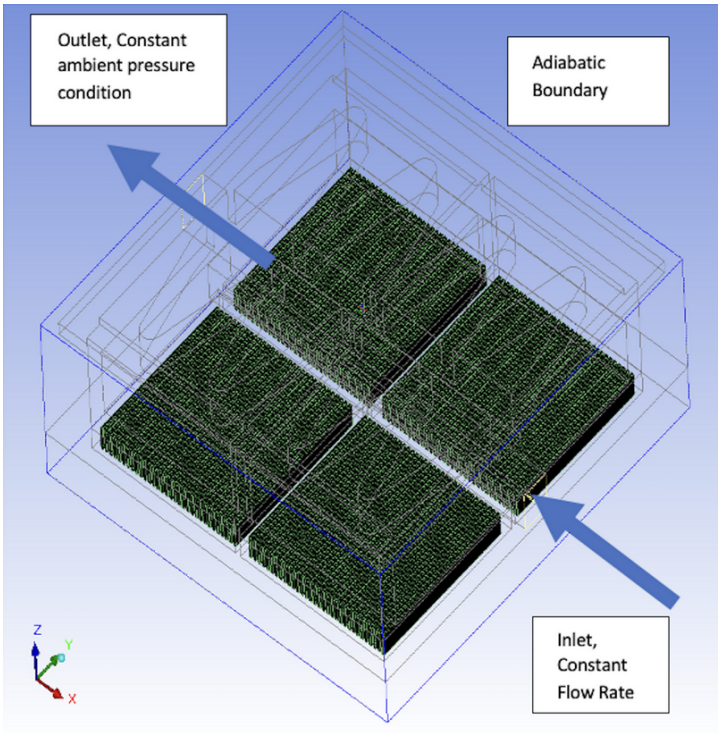

FIG. 7: Summary of the boundary conditions used for the CFD simulations

Energy conservation:

$$\frac{d}{dt}(\rho h) + \nabla.(\rho h v) = \nabla[(k + k_t)\nabla T] + S_h \tag{3}$$

where k and k_t are the molecular and turbulent transport conductivity, and S_h is a term that includes heat sources due to volumetric definitions. Ansys Icepak involves simple conductive equations to solve solid conduction models which can be written as follows:

$$\frac{d}{dt}(\rho h) = \nabla.(k\nabla T) + S_h \tag{4}$$

In this equation k represents thermal conductivity, T is the temperature, h is enthalpy (sum of flow energy and internal energy), and ρ is the density.

4. RESULTS

The results reviewed in this section are divided into two parts: results for cold pate without bimetal strips (baseline simulations) and CFD results with bimetal strips added to the cold plate. A summary of different cases in terms of source power simulated is shown in Table 3. The heat source in the CFD simulations is modeled as a 2D heat source with a user-defined power value as shown in Fig. 8. The total heat dissipation value has been chosen to represent the future experimental work that will be carried out to validate this numerical study. The value of 10 W

TABLE 3: No bimetal—top surface temperature at 1 lpm for all cases

Zone No.	Temperatures at 1 lpm—No bimetal (°C)				
	Case 1	Case 2	Case 3	Case 4	Case 5
Zone 1	29.2	26.0	28.4	26.0	28.3
Zone 2	30.7	26.5	29.9	27.7	28.8
Zone 3	30.7	26.2	29.8	28.7	28.0
Zone 4	34.9	28.1	32.9	32.2	29.3
Zone 5	39.8	30.0	37.9	35.7	30.7
Zone 6	43.1	33.0	38.7	38.3	32.7
Zone 7	38.7	36.1	29.6	29.9	35.7
Zone 8	34.7	32.6	27.9	28.6	31.7
Zone 9	30.1	28.7	26.5	27.0	27.7
Zone 10	29.6	28.3	25.6	27.5	27.5
Zone 11	29.8	29.0	26.3	28.5	26.8
Zone 12	28.6	27.9	25.9	27.7	26.1

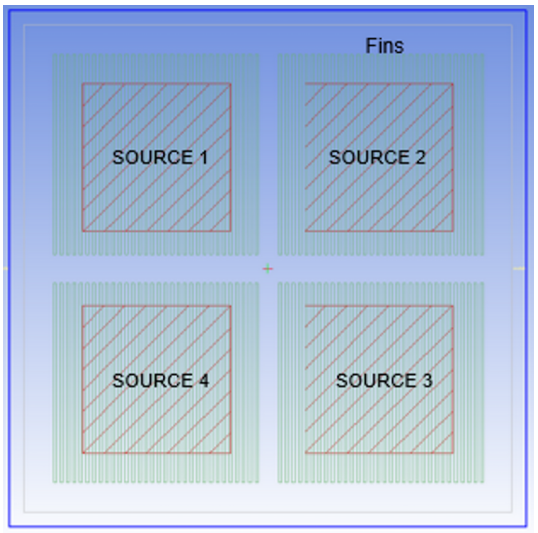

FIG. 8: 2D heat sources modeled in Ansys Icepack to represent nonhomogeneous thermal profile on a chip

represents the idle processor workload condition, which is typically around 10% of the total TDP of processors. Each heat source is symmetrically located under each fin cavity section, below the cold plate base. Five different cases were simulated for the cold plate with bimetal (WB) and without bimetal (NB). A minimum source power of 10 W and a maximum source power of 90 W were used in different combinations with five different inlet flow rates between the range of 0.6 lpm to 1.5 lpm with an increment of 0.3 lpm.

4.1 CFD Results for No-Bimetal Condition

The first set of simulations of the cold plate design was done with a no-bimetal (NB) condition as a baseline design case for the cold plate. The results from each of the five cases as described

in Table 4 of NB simulations at a 1 lpm coolant flow rate. The temperature at the top surface of the middle plate was also captured for temperature input of bimetal deflection value. Figure 9 represents different zones defined to capture top surface coolant temperature for bimetal deflection. As explained in the previous example of the simulation procedure, these zone temperatures will predict the deflection of the bimetal accurately at an instance. Table 5 represents the different zone temperatures for the bimetal at the 1 lpm coolant flow rate case. A similar trend in the temperature was observed for all other flow rates. The temperature contours, as seen in Fig. 10, show that temperature values for Source 2 and Source 3 are large as compared to the other two. This was also noted for the other flow rate cases that were simulated. The possible explanation for this behavior is that the coolant enters the cold plate from right to left, as seen in Fig. 10. This

TABLE 4: Different power conditions for each heat source for the CFD analysis

	Source 1	Source 2	Source 3	Source 4
Case 1	90 W	90 W	90 W	90 W
Case 2	10 W	10 W	90 W	90 W
Case 3	90 W	90 W	10 W	10 W
Case 4	10 W	90 W	10 W	90 W
Case 5	90 W	10 W	90 W	10 W

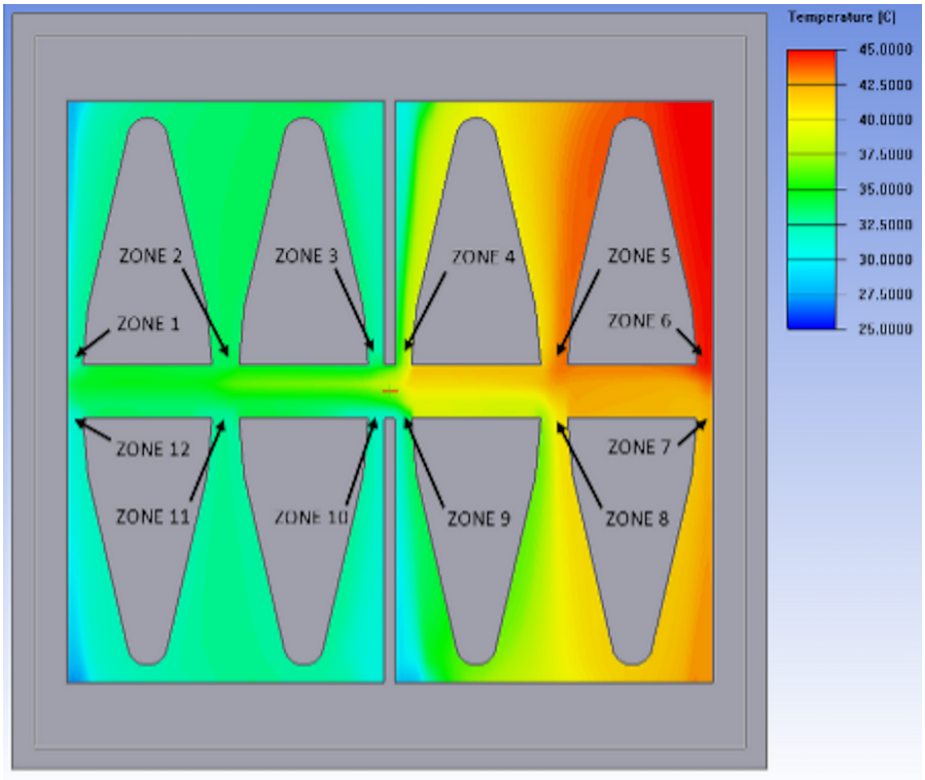

FIG. 9: Locations of the zone defined for temperature probes in the CFD model

causes better flow movement and a more uniform distribution in the fin sections for Sources 1 and 4. Hence, as seen in the thermal profiles, there is a lower temperature distribution in those fin sections. CFD data shows that the difference in source temperature for the baseline case was approximately 12°C as seen from the data in Table 5 for the NB condition in Case 1 when all the heat sources are at peak power values. When the power value to two of the sources is reduced to 10 W, the temperature difference among the sources still stays at approximately 12°C for the NB condition. The maximum temperature difference of approximately 16.7°C occurs between the heat sources for Case 3 where the heat sources of the same power dissipation are located on either side of the inlet section.

4.2 CFD Results Comparison between No-Bimetal and With-Bimetal Cases

After performing all the simulations for no bimetal condition on the cold plate for different power distribution conditions at different lpm, simulations for the case after integrating the bimetal were performed. Because the simulation in the software tool are only conjugate heat transfer simulations and structural movement cannot be simulated, a way to replicate the motion of the bimetal strip was used. This was done by creating blocks that represent the same percentage of open area at any given temperature as the bimetal strips. As an example, if the bimetal strip allows a 3 × 3 mm area for the coolant to pass through at 35°C, the same can be created by using 3D blocks that allow the same area for the coolant to pass through.

Figure 10 shows a comparison of the temperatures on the base of the cold plate for Case 1 at 1 lpm. Similar temperature behavior was seen at all other coolant inlet flow rate conditions. It was observed that the implementation of the bimetal strip or the dynamic cold plate design significantly reduces the difference in the temperature distribution on the base of the baseline cold plate design. Table 5 shows a comparison between source temperatures between the baseline cold plate design against the dynamic cold plate design with bimetal. Figure 11 shows the comparison of the temperature difference across the base of the cold plate for all the cases with and without bimetal. A maximum reduction of up to 60% in the temperature difference of the base plate was seen, and this is further evaluated by calculating the thermal resistance value for each case. This shows that the proposed dynamic cold plate design using bimetal strips can significantly improve the temperature homogeneity on the case surface of high-power CPUs or GPUs. An improvement in this temperature distribution can also be vital in enhancing the reliability of these devices and preventing failures caused due to temperature nonuniformity on and around chip surfaces.

To calculate the Rth value for each case the following equation was used:

TABLE 5: Source temp comparison, no bimetal versus with bimetal at 1 lpm

Case No.	Flow rate (1 lpm)								Delta T (°C)	
	Source 1 (°C)		Source 2 (°C)		Source 3 (°C)		Source 4 (°C)			
	NB	WB	NB	WB	NB	WB	NB	WB	NB	WB
Case 1	37.9	37.3	48.9	40.6	46.6	41.8	36.7	37.1	12.2	4.7
Case 2	28.1	27.7	33.3	29.5	42.6	37.2	35.4	35.5	14.5	9.5
Case 3	36.6	35.6	44.9	36.4	33.5	29.1	28.2	27.7	16.7	8.7
Case 4	30.8	36.5	44.0	36.7	33.5	29.3	34.6	27.7	13.1	8.9
Case 5	35.4	35.4	33.6	29.9	42.0	37.3	29.9	29.1	12.2	8.2

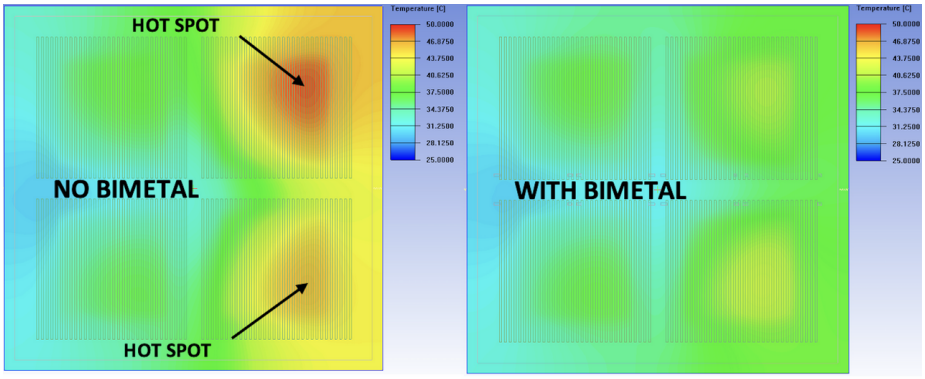

FIG. 10: Comparison of the temperature contours for Case 1: (a) showing the base temperature for cold plate without bimetal; and (b) with bimetal (dynamic cold plate case)

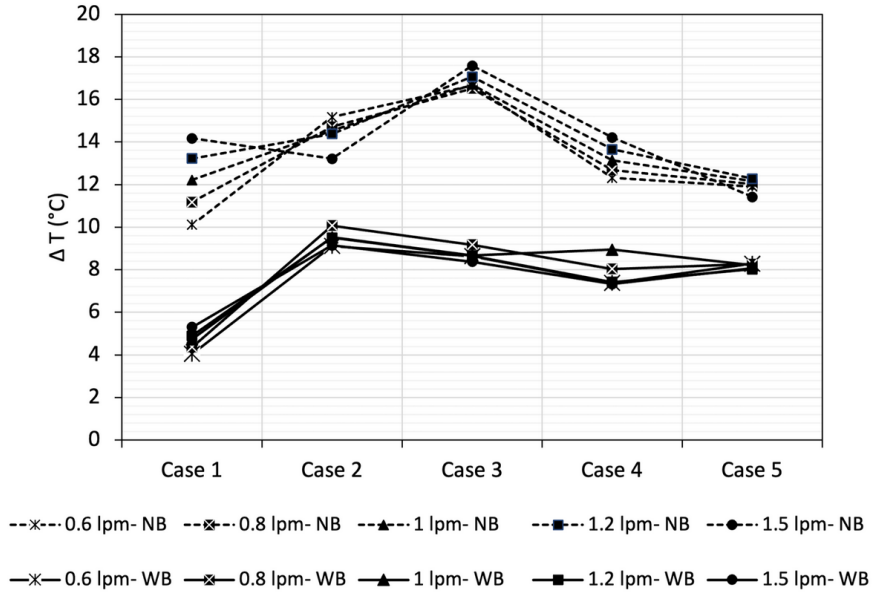

FIG. 11: Variation of the temperature difference across the cold plate for all cases at different coolant lpm for the baseline cold plate and dynamic cold plate

$$R_{th} = \frac{(T_{base} - T_{in})}{Q} \tag{5}$$

where T_{base} is taken from the average of the base temperature at each case, and T_{in} is the water inlet temperature, which is 25°C for all the cases. Q represents the total load applied on the cold plate and is taken from Table 4 for the respective case. Figure 12 represents thermal resistance variation for different power distribution cases between the baseline cold plate design and the dynamic cold plate design. It was observed that up to 42% of the reduction in the thermal resistance value can be achieved by implementing dynamic control of the flow at the cold plate level. A comparison of the variation of the thermal resistance trend for the baseline cold plate

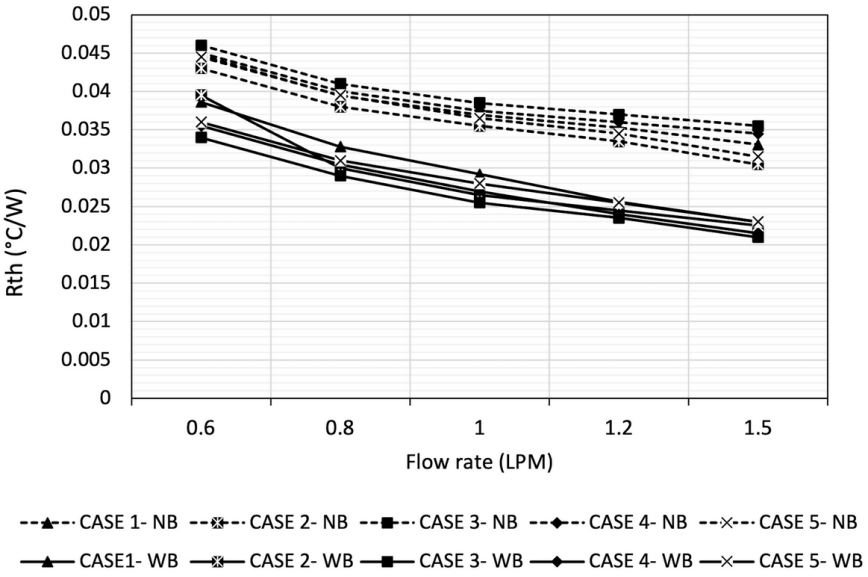

FIG. 12: Variation of the thermal resistance for the baseline and dynamic cold plate design at different lpm

design and dynamic cold plate also shows that the difference in the thermal resistance values converges at higher flow rates for the dynamic cold plate designs. The same trend is the opposite for the baseline cold plate design without bimetal strips.

5. CONCLUSION AND FUTURE WORK

As the power densities at the chip level continue to increase due to higher processing demands, data center administrators are moving toward liquid-based cooling technologies for better thermal management. Direct-to-chip liquid cooling using cold plates allows easy retrofitting in air-cooled servers and can be used to dissipate very high heat fluxes. However, the challenge of nonuniform heat distribution over the chip surface persists, which has been addressed in this study by proposing a dynamic cold plate design. An in-depth numerical study was conducted for design optimization of the fin geometry and selection of the best-suited bimetals to be integrated inside the cold plate. The results of thermal enhancement using the dynamic cold plate were discussed by comparing the pressure drop, thermal resistance, and temperature difference across the inlet and the outlet with the baseline design of the cold plate.

The results obtained from the comparison of the proposed dynamic cold plate to the baseline design show that a reduction of a minimum of 30% to a maximum of 62% is achieved in the value of temperature gradient across the cold plate. This reduction in the thermal gradient on the cold plate base also leads to a reduction of up to a maximum of 40% in the thermal resistance value of the cold plate. Studies have shown that temperature causes as much as 55% of failures in electronic devices. It can thus be hypothesized that by implementing the proposed cold plate design this significant improvement in the base temperature also directly affects the thermal resistance value of the cold plate, which was found to be reduced by 40%. As discussed previously, temperature and thermal mismatches are among the primary causes of failures among electronic devices. It can be postulated from the results obtained using CFD that

some package-level reliability enhancement can be expected by implementing the proposed cold plate solution. However, this would require a significant experimental testing effort to quantify the improvement. The authors are actively working on more bimetal strip designs and materials to obtain comparisons for the best possible dynamic cold plate design. Work is also being done to automate the opening area of the cold plate using a MATLAB code integrated with a commercial data center CFD tool, 6SigmaET. This will allow visualization of the dynamic response of the cold plate to a local hotspot and generate more accurate results in terms of performance enhancement of the cold plate. Different inlet and outlet configurations are also being studied using numerical analysis. The final cold plate design will be manufactured for validation of the CFD data.

REFERENCES

Ansys, Icepak, Release 2019R3, Ansys Icepak User's Guide, Ansys, Inc., 2019.

Ariyo, D.O. and Bello-Ochende, T., Constructal Design of Two-Phase Stacked Microchannel Heat Exchangers for Cooling at High Heat Flux, *Int. Commun. Heat Mass Transf.*, vol. **125**, p. 105294, 2021.

Bailey, C., Thermal Management Technologies for Electronic Packaging: Current Capabilities and Future Challenges for Modelling Tools, in *Proc. 10th Electronics Packaging Technology Conf.*, pp. 527–532, 2008.

Chauhan, A., Sammakia, B., Ghose, K., Ahmed, G.R., and Agonafer, D., Hot Spot Mitigation Using Single-Phase Microchannel Cooling for Microprocessors, in *Proc. 12th IEEE Int. Conf., Thermal and Thermomechanical Phenomena in Electronic Systems (ITherm)*, June 2–5, Las Vegas, NV, 2010.

Dias, R. and Skoglund, L., Variable Depth Microchannels, US Patent Application US20080073061A1, filed on September 27, 2006, published on March 27, 2008.

Engineered Material Solutions, Data Sheets, n.d., Accessed August 10, from https://www.emsclad.com/downloads/data-sheets.html, 2021.

Goodson, K., Kenny, T., Zhou, P., Upadhya, G., Munch, M., McMaster, M., and Horn, J., Method and Apparatus for Achieving Temperature Uniformity and Hot Spot Cooling in a Heat Producing Device, Cooligy Inc., US Patent 7,104,312, B2, filed October 30, 2003, issued September 12, 2006.

Hegde, P.G. and Seetharamu, K.N., Effects of Non-Uniform Base Heating in Multi Stack Microchannel Heat Sinks Used for Cooling High Heat Flux Electronic Chips and Devices, in *Electronic Manufacturing Technology Symp. (IEMT) 33rd IEEE/CPMT*, November 4–6, Penang, Malaysia, 2008.

Hoang, C.H., Rangarajan, S., Manaserh, Y., Tradat, M., Mohsenian, G., Choobineh, L., Ortega, A., Schiffres, S., and Sammakia, B., A Review of Recent Developments in Pumped Two-Phase Cooling Technologies for Electronic Devices, *IEEE Trans. Comp. Pack. Manufact. Technol.*, vol. **11**, no. 10, pp. 1565–1582, 2021.

Kandlikar, S.G. and Hayner, C.N., Liquid Cooled Cold Plates for Industrial High-Power Electronic Devices—Thermal Design and Manufacturing Considerations, *Heat Transf. Eng.*, vol. **30**, no. 12, pp. 918–930, 2009.

Kasukurthy, R., Challa, P.S., Palanikumar, R.R., Manimaran, B.R., and Agonafer, D., Flow Analysis and Linearization of Rectangular Butterfly Valve Flow Control Device for Liquid Cooling, in *Proc. 17th IEEE Intersociety Conf. on Thermal and Thermomechanical Phenomena in Electronic Systems (ITherm)*, pp. 683–687, 2018.

Khattak, Z. and Ali, H.M., Air Cooled Heat Sink Geometries Subjected to Forced Flow: A Critical Review, *Int. J. Heat Mass Transf.*, vol. **130**, pp. 141–161, 2019.

Kumar, A., Shahi, P., and Saha, S.K., Experimental Study of Latent Heat Thermal Energy Storage System

for Medium Temperature Solar Applications, in *Proc. 4th World Congress on Mechanical, Chemical, and Material Engineering (MCM'18)*, Madrid, Spain, August 16–18, Paper No. HTFF 152, 2018.

Lee, Y.J., Lee, P.S., and Chou, S.K., Hot Spot Mitigating Oblique Finned Microchannel Heat Sink, *Int. Mech. Eng. Congress Exp.*, November 12–18, Vancouver, BC, Canada, 2010.

Lee, Y.J., Lee, P.S., and Chou, S.K., Hotspot Mitigating with Obliquely Finned Microchannel Heat Sink—An Experimental Study, *IEEE Trans. Comp. Pack. Manufact. Technol.*, vol. **3**, no. 8, pp. 1332–1341, 2013.

Li, Z. and Kandlikar, S.G., Current Status and Future Trends in Data-Center Cooling Technologies, *Heat Transf. Eng.*, vol. **36**, no. 6, pp. 523–538, 2015.

Li, J., Peterson, G.P., and Cheng, P., Three-Dimensional Analysis of Heat Transfer in a Micro-Heat Sink with Single Phase Flow, *Int. J. Heat Mass Transf.*, vol. **47**, no. 19, pp. 4215–4231, 2004.

Lu, M.C. and Wang, C.C., Effect of the Inlet Location on the Performance of Parallel-Channel Cold-Plate, *IEEE Trans. Comp. Pack. Manufact. Technol.*, vol. **29**, no. 1, pp. 30–38, 2006.

Niazmand, A., Chauhan, T., Saini, S., Shahi, P., Bansode, P.V., and Agonafer, D., CFD Simulation of Two-Phase Immersion Cooling Using FC-72 Dielectric Fluid, in *Proc. ASME 2020 Int. Technical Conf. and Exhibition on Packaging and Integration of Electronic and Photonic Microsystems*, October 27–29, 2020a.

Niazmand, A., Murthy, P., Saini, S., Shahi, P., Bansode, P., and Agonafer, D., Numerical Analysis of Oil Immersion Cooling of a Server Using Mineral Oil and Al_2O_3 Nanofluid, in *Proc. of the ASME 2020 Int. Technical Conf. and Exhibition on Packaging and Integration of Electronic and Photonic Microsystems*, Virtual, Online, October 27–29, 2020b.

Prasher, R. and Chang, J.Y., Cooling of Electronic Chips Using Microchannel and Micro-Pin Heat Exchangers, in *Proc. 6th Int. ASME Conf. on Nanochannels, Microchannels and Minichannels, ICNMM2008*, June 23–25, Darmstadt, Germany, 2008.

Qu, W. and Mudawar, I., Analysis of Three-Dimensional Heat Transfer in Micro-Channel Heat Sinks, *Int. J. Heat Mass Transf.*, vol. **45**, no. 19, pp. 3973–3985, 2002.

Saini, S., Adsul, K.K., Shahi, P., Niazmand, A., Bansode, P., and Agonafer, D., CFD Modeling of the Distribution of Airborne Particulate Contaminants inside Data Center Hardware, in *Proc. of the ASME 2020 Int. Technical Conf. and Exhibition on Packaging and Integration of Electronic and Photonic Microsystems*, Virtual, October 27–29, 2020a.

Saini, S., Shah, J.M., Shahi, P., Bansode, P., Agonafer, D., Singh, P., Schmidt, R., and Kaler, M., Effects of Gaseous and Particulate Contaminants on Information Technology Equipment Reliability—A Review, *ASME J. Electron. Packag.*, vol. **144**, no. 3, p. 030801, 2022.

Saini, S., Shahi, P., Bansode, P., Siddarth, A., and Agonafer, D., CFD Investigation of Dispersion of Airborne Particulate Contaminants in a Raised Floor Data Center, in *Proc. 36th Semiconductor Thermal Measurement, Modeling & Management Symposium (SEMI-THERM)*, San Jose, CA, USA, pp. 39–47, 2020b.

Shahi, P., Agarwal, S., Saini, S., Niazmand, A., Bansode, P., and Agonafer, D., CFD Analysis on Liquid Cooled Cold Plate Using Copper Nanoparticles, in *Proc. of the ASME 2020 Int. Technical Conf. and Exhibition on Packaging and Integration of Electronic and Photonic Microsystems*, Virtual, October 27–29, 2020.

Shahi, P., Deshmukh, A., Hurnekar, H., Saini, S., Bansode, P.V., Kasukurthy, R., and Agonafer, D., Design, Development, and Characterization of a Flow Control Device for Dynamic Cooling of Liquid-Cooled Servers, *ASME J. Electron. Packag.*, vol. **144**, no. 4, p. 041008, 2022.

Shahi, P., Saini, S., Bansode, P., and Agonafer, D., A Comparative Study of Energy Savings in a Liquid-Cooled Server by Dynamic Control of Coolant Flow Rate at Server Level, *IEEE Trans. Comp. Pack. Manufact. Technol.*, vol. **11**, no. 4, pp. 616–624, 2021.

Sharma, C.S., Schlottig, G., Brunschwiler, T., Tiwari, M.K., Michel, B., and Poulikakos, D., A Novel Method of Energy Efficient Hotspot-Targeted Embedded Liquid Cooling for Electronics: An Experimental Study, *Int. J. Heat Mass Transf.*, vol. **88**, pp. 684–694, 2015.

Wei, X., Stacked Microchannel Heat Sinks for Liquid Cooling Microelectronics Devices, PhD, Georgia Institute of Technology, 2004.

Xie, G., Li, S., Sunden, B., and Zhang, W., Computational Fluid Dynamics for Thermal 14 Performance of a Water-Cooled Minichannel Heat Sink with Different Chip Arrangements, *Int. J. Numer. Methods Heat Fluid Flow*, vol. **24**, no. 4, pp. 797–810, 2014.